Available online at www.sciencedirect.com

ScienceDirect

Procedia CIRP 143 (2026) 813–816

www.elsevier.com/locate/procedia

14th CIRP Conference on Photonic Technologies

Laser ablation for the recovery of $LiFePO_4$ cathode active material from aluminum current collectors in Li-ion batteries

Riccardo Cesaro[a,*], Eugenio Gibertini[b], Luca Magagnin[b], Ali Gökhan Demir[a]

[a]*Department of Mechanical Engineering, Politecnico di Milano, Via La Masa 1, 20156 Milan, Italy*
[b]*Department of Chemistry, Materials and Chemical Engineering "Giulio Natta", Politecnico di Milano, Via Bassini 6, 20131 Milano, Italy*

* Corresponding author. Tel.: +39 02 23998593. *E-mail address:* riccardo.cesaro@polimi.it

Abstract

The increasing demand for lithium-ion batteries, driven by the automotive and renewable energy storage sectors, calls for the development of strategies to minimize raw material waste during both manufacturing and end-of-life stages. This need is particularly relevant for chemistries such as LFP, which are gaining attention due to their safety, low cost, and growing market share. This work investigates the feasibility of selectively removing $LiFePO_4$ cathode active material from aluminum current collectors using a nanosecond pulsed fiber laser. Ablation parameters were varied to identify a suitable process window enabling uniform coating removal while preserving the substrate integrity. The recovered powder was collected in a controlled atmosphere setup and characterized by SEM and EDS analyses, alongside the processed electrode surfaces. Selective ablation was achieved under conservative parameter sets, producing predominantly spherical particles with approximately 1-10 µm diameter. The results highlight the potential of conventional nanosecond laser systems for direct recycling and remanufacturing strategies.

Keywords: Lithium-ion batteries; Laser ablation; Material separation; Direct recycling.

1. Introduction

The demand for batteries is expected to increase significantly in the coming years, mainly driven by the automotive sector and renewable energy storage applications [1]. As a consequence, the development of more efficient and sustainable technologies for both battery manufacturing and end-of-life management is becoming increasingly important. In particular, minimizing raw material waste should represent a primary driving force, especially for countries that rely heavily on external resource supply.

Lithium-ion batteries currently offer one of the best compromises in terms of energy density, safety, and cycle life, and are available in different chemistries (e.g., NMC, LFP, LCO) as well as various formats (pouch, cylindrical, prismatic) [2]. Despite these variations, they share a similar electrode architecture and comparable large-scale manufacturing processes.

Laser-based processes enable fast and highly localized material processing with excellent accuracy and virtually no tool wear, particularly when remote scanning systems are used [3].

As the cost of pulsed laser sources continues to decline and higher peak powers become available, their application can extend beyond conventional processes, opening new possibilities for controlled material interaction [4, 5] and selective removal [6]. Such approaches may be exploited to recover active materials from current collectors in end-of-life batteries as an alternative to conventional pyrometallurgical or hydrometallurgical methods [7, 8].

Few studies have investigated alternative processes capable of selectively separating active materials from current

10.1016/j.procir.2026.07.171

collectors [9, 10], even though such approaches could significantly enhance recycling feasibility, particularly for cathode chemistries that do not contain high-value critical metals, such as LFP.

In this preliminary study, the feasibility of using pulsed laser ablation for the separation of LFP cathode active material from the aluminum current collector is investigated. The aim is to identify suitable processing parameters enabling effective material removal while preserving the integrity of the metallic substrate.

2. Experimental Setup

2.1. Input material

The selected material is a commercially available single-side coated aluminum foil cathode (MSE Supplies LLC, Tucson, AZ, USA), in which the active material is Lithium Iron Phosphate ($LiFePO_4$). The electrodes were delivered in a vacuum-sealed package containing five sheets of 260 × 230 mm^2. The electrode thickness, independently measured with a linear measurement system, ranged from approximately 82 µm at the edges to 84 µm in the central region. This 2 µm variability may affect ablation repeatability. According to the manufacturer, the specific capacity of the active material is 135 mAh/g. The product specifications are summarized in Table 1. For the ablation experiments, the never-cycled electrodes were sectioned into smaller samples areas 32 × 22 mm^2.

Table 1. Specifications of the LFP electrode used for the experiments.

Material Specification	Value
Electrode type	LFP cathode
Coated area	260x200 mm
Aluminum thickness	15 µm
Coating thickness	67-69 µm
Coating area density	14 mg/cm^2
Active material wt.%	94%
PVDF5130 binder wt.%	3.5%

2.2. Laser system

The optical source employed in this study is a near-infrared, nanosecond pulsed IPG fiber laser. The system operates at pulse repetition rates up to 80 kHz, with a fixed pulse duration of 250 ns. A maximum pulse energy of 1020 µJ is available within the 20–50 kHz repetition rate range.

The beam is delivered through a two-axis galvanometric scanning head (TSH 8310, Sunny Technology, Beijing, China), and an F-theta lens with a focal length of 100 mm (SL-1064-70-100, Wavelength Opto-Electronic, Ronar-Smith, Singapore), enabling planar processing with scanning speeds up to 6000 mm/s over a maximum working field of 70 × 70 mm^2. With a collimated beam diameter of 5.9 mm, the resulting minimum focal spot diameter is approximately 39 µm at the focal plane. The main optical parameters of the laser system are summarized in Table 2.

The laser beam exhibits a quasi-Gaussian intensity profile. Under maximum pulse energy conditions, the peak pulse power reaches 9 kW. At focus, this corresponds to a peak intensity of $1.5 \cdot 10^9$ W/cm^2 and a peak fluence of 167 J/cm^2.

Table 2. Laser system characteristics.

System Specification	Value
Source brand and model	IPG YLP-1/100/50/50
Architecture	Fiber, Q-switched
Wavelength	1064 nm
Max. average power	54 W
Pulse repetition rate	20-80 kHz
Max. pulse energy	1.02 mJ
Pulse duration	250 ns
Beam quality factor, M^2	1.7
Collimated beam diameter	5.9 mm
Focal length	100 mm
Calculated diameter at focal point	39 µm
Rayleigh length	0.66 mm

2.3. Powder collection system

All experiments were conducted in the laboratory-scale setup schematically shown in Fig. 1. To ensure safe operation of the ablation process and enable subsequent powder collection, a dedicated enclosed system was designed and fabricated. The processing chamber consists of a custom 3D-printed PLA enclosure with external dimensions of 102 × 102 mm^2. To prevent external aluminum contamination and ensure mechanical stability, all metallic components were manufactured from stainless steel, including the fastening screws, the laser-cut lid, and the sample holder.

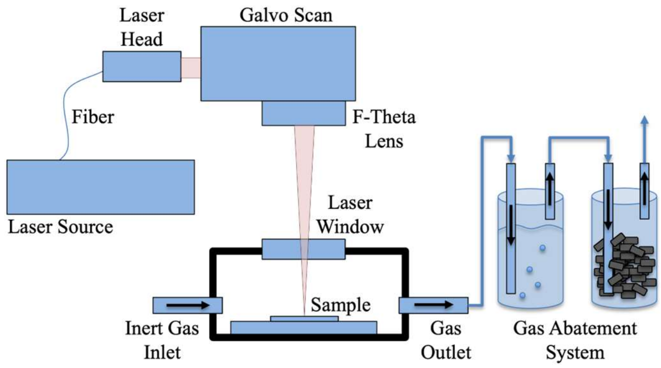

Fig. 1. Schematic of the experimental laser ablation setup.

To enable laser transmission into the chamber, an optical window (N-BK7, Ø50 mm, 4 mm thick, 45 mm clear aperture, V-coated for 1064 nm, λ/4 flatness; Edmund Optics, Barrington, NJ, USA) was integrated. The induced focal shift was estimated to be ~1.34 mm via paraxial approximation (n = 1.506 at 1064 nm) and compensated during the experiments.

A constant flow of molecular nitrogen was supplied to the chamber during processing to minimize oxidation of the ablated powder, maintaining a slight overpressure (2 bar inlet) to compensate for pressure losses across the filter and gas abatement system. The ablated powder was primarily retained on a paper filter positioned on the gas outlet and was subsequently recovered by gentle mechanical scraping.

Thermal degradation of PVDF binder occurs above approximately 316 °C, mainly through dehydrofluorination reactions [11]. To mitigate the release of hazardous by-products such as hydrogen fluoride (HF) and fluorinated organic compounds ($C_xF_yH_z$,with $x \geq 2$), appropriate gas treatment measures were implemented. Specifically, the exhaust stream was bubbled through a 1 M NaOH solution for acid neutralization, followed by filtration through activated carbon to adsorb residual organic species.

2.4. Experimental design

The objective of this study is to evaluate the feasibility of selectively ablating the cathode active material while preserving, as much as possible, the integrity of the underlying aluminum current collector. Achieving this requires uniform surface scanning under controlled conditions, taking into account factors such as thermal effects, material absorption characteristics, and inherent limitations of the experimental setup.

To systematically investigate the process window, an array of square patterns (5 × 5 mm^2) was defined on the electrode surface. The squares were spaced 1 mm apart, and a minimum delay of 5 s was introduced between consecutive scans to reduce thermal interaction and heat accumulation between adjacent test areas. Each square was processed using a linear hatching strategy with bidirectional scanning.

The investigated process parameters were the scanning speed (v) and the average laser power (P), while maintaining a fixed pulse repetition rate of 50 kHz. This operating frequency was selected because it provides both the maximum average power and the maximum pulse energy available for the system.

All experiments were conducted at the focal position. Two hatch distances (d_h) were considered in order to evaluate the effect of pulse overlap in the transverse direction: 0.05 mm and 0.03 mm. These values were selected to represent, respectively, a hatch spacing slightly larger and slightly smaller than the nominal focal spot diameter (39 µm), thereby enabling different degrees of surface coverage and energy accumulation. Both single-pass (N=1) and double-pass (N=2) strategies were investigated. In the double-pass configuration, the second scan was performed using the same process parameters as the first to assess the effect of repeated irradiation and enhanced material removal.

To minimize edge overprocessing caused by scanner acceleration and deceleration at the beginning and end of each scan line, a laser-on/off delay of 100 µs was implemented.

For each condition, 8 scanning speeds and 3 power levels were tested, resulting in a total of 96 parameter combinations.

3. Results

3.1. Ablation strategy

The $LiFePO_4$-based active material was readily removed using near-infrared laser irradiation. Under the investigated conditions, the coating was always fragmented into fine particulate matter that was efficiently transported within the process atmosphere. No noticeable melting, sticking behavior, or visible discoloration occurred.

However, as the ablation front approached the underlying aluminum current collector, the process window became significantly narrower. The transition between complete coating removal and substrate damage was found to be critical (Fig. 2). From a recycling perspective, even minor aluminum contamination in the collected powder would be highly detrimental, particularly in view of potential direct reuse routes.

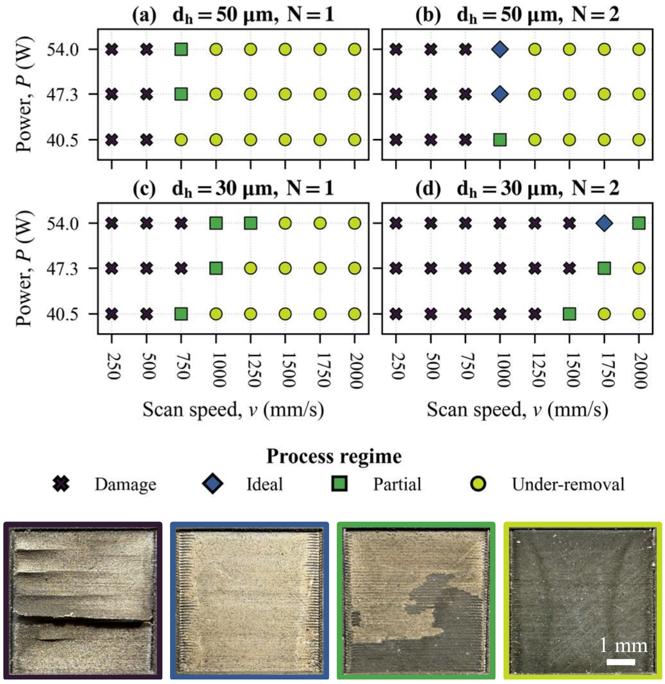

Fig. 2. Feasibility map illustrating the effect of the investigated laser parameter sets. The insets highlight four representative ablation outcomes.

The conditions identified as ideal resulted in complete exposure of the aluminum current collector, which remained macroscopically smooth and reflective, with no evident signs of surface texturing. In some intermediate parameter combinations, only localized exposure of the aluminum substrate was observed, as summarized in Fig. 3, which reports the removal percentage of the active layer evaluated by image processing techniques.

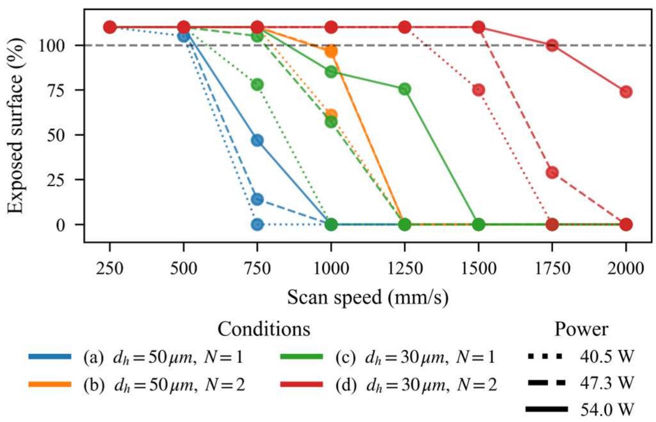

Fig. 3. Exposed surface percentage for all experimental conditions, plotted together for trend comparison. Values above 100 % indicate partial or complete damage of the substrate by the laser.

Among the tested conditions, a single configuration (P = 54 W, v = 1250 mm/s, d_h = 0.03 mm, N = 1) led to localized delamination of the coating from the substrate. This phenomenon significantly enhanced the separation efficiency, as the active layer detached in large fragments rather than being progressively ablated. However, this behavior was not easily reproducible across the processed areas.

For the subsequent material characterization analyses, a more conservative and stable parameter set was selected (P = 54 W, v = 1000 mm/s, d_h = 0.05 mm, N = 1). Under these conditions, a thin residual coating layer always remained on the aluminum surface, ensuring minimal interaction with the substrate, thus maintaining process repeatability.

3.2. Material characterization

SEM imaging of the electrode surfaces before and after laser treatment (Fig. 4a and 4b, respectively) showed that the processed areas remained largely planar, with no significant surface alterations, grooves, or irregularities. This indicates that the active material responds well to the laser, and that the selected scanning strategy and hatch spacing enable uniform removal.

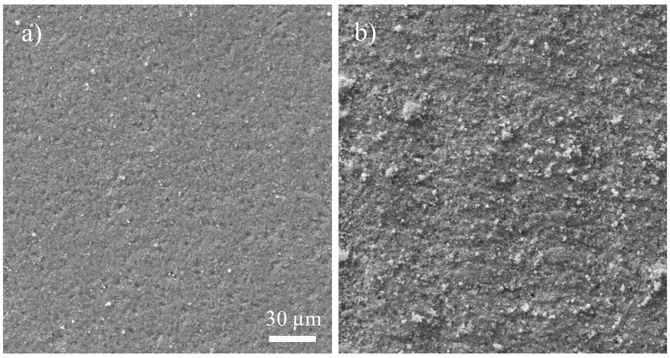

Fig. 4. SEM images of the electrode surface a) before and b) after ablation (P = 54 W, v = 1000 mm/s, d_h = 0.05 mm, N = 1).

The ablated material consisted of particles that tended to be roughly spherical, with sizes predominantly ranging from 1 to 10 µm, as observed by SEM imaging (Fig. 5). Elemental composition was assessed using EDS, both at discrete points and over selected areas. Comparison with EDS measurements of the original, unablated electrode coating allowed verification of the relative elemental ratios and confirmed the absence of macroscopic aluminum contamination from the underlying layers (Table 3).

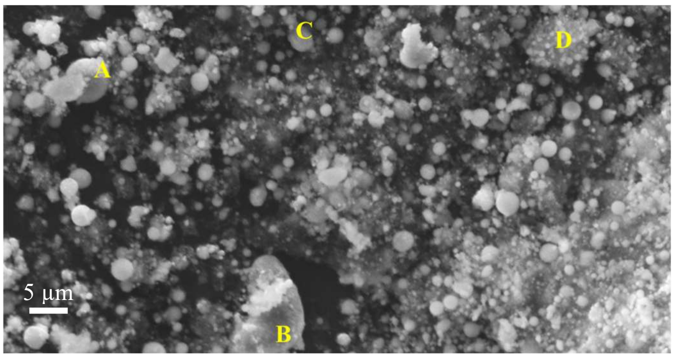

Fig. 5. SEM image of the collected powder showing the EDS analysis points.

Table 3. Normalized elemental composition obtained from EDS analysis.

Position	O (at%)	P (at%)	Fe (at%)	Al (at%)
A	28.70	31.10	40.20	0.00
B	67.18	16.98	15.84	0.00
C	58.63	21.28	20.09	0.00
D	60.34	23.45	16.21	0.00
Powder (area)	61.82	20.19	17.99	0.00
Pristine coating (area)	51.20	25.23	23.57	0.00

4. Conclusions

Selective ablation of the active material from LFP electrodes was successfully achieved using a simple and cost-effective nanosecond laser system. This approach opens promising perspectives for direct remanufacturing and material reuse, contributing to waste reduction in battery recycling. Further work should address the underlying ablation mechanisms and evaluate the process energy consumption against conventional techniques. Moreover, the electrochemical properties of the recovered powder need to be assessed to determine its practical suitability for full or partial reintegration into new battery electrodes with minimal additional processing.

References

[1] Fleischmann, J., Hanicke, M., Horetsky, E., Ibrahim, D., Jautelat, S., Linder, M., Schaufuss, P., Torscht, L., van de Rijt, A., 2023. Battery 2030: Resilient, sustainable, and circular. McKinsey & Company 16, 2023.

[2] Stoyanov, S., Gueorgiev, V., 2025. Comparative Analysis of Lithium-Ion Batteries, in: 2025 19th Conference on Electrical Machines, Drives and Power Systems (ELMA). Presented at the 2025 19th Conference on Electrical Machines, Drives and Power Systems (ELMA), IEEE, Sofia, Bulgaria, pp. 1–5.

[3] D'Arcangelo, S., Busatto, M., Caprio, L., Previtali, B., Demir, A.G., 2024. Hybrid use of a robotic welding system in remote laser separation of thin-sheet Al casings for the recycling of battery packs. Journal of Laser Applications 36, 032023.

[4] Sun, X., Wang, L., Yu, D., Zhang, J., Wang, W., Mei, X., 2026. Laser Processing of 3D Electrodes for High-Performance Metal-ion Batteries. Advanced Materials e19582.

[5] Sahoo, S.S., Narayan, J., Narayan, R.J., Sun, X.-G., Paranthaman, M.P., 2025. Enhancement of the electrochemical performance of LiFePO4 cathode material by nanosecond laser annealing. MRS Commun. 15, 255–264.

[6] Kriegler, J., Ballmes, H., Dib, S., Demir, A.G., Hille, L., Liang, Y., Wach, L., Weinmann, S., Keilhofer, J., Kim, K.J., Rupp, J.L.M., Zaeh, M.F., 2024. Surface Reconditioning of Lithium Metal Electrodes by Laser Treatment for the Industrial Production of Enhanced Lithium Metal Batteries. Adv Funct Materials 34, 2313766.

[7] Cao, N., Zhang, Y., Gu, X., Wu, M., 2025. Efficient recycling of spent Li-ion battery cathodes by laser-induced high-temperature thermal shock. Nat Commun 16, 7169.

[8] Wang, Z., Hu, X., Zhang, H., Song, Y., Yao, Y., Huang, Y., 2025. Battery Cathode Recycling With Superior Dissolution Kinetics by Laser Augmentation. Small Methods 9, 2401975.

[9] Tancin, R.J., Özdoğru, B., Dutta, N.S., Finegan, D.P., Tremolet De Villers, B.J., 2024. Direct reuse of graphite and lithium nickel manganese cobalt oxide (NMC) recovered from ultrafast-laser ablation debris in Li-ion battery electrodes. Journal of Power Sources 596, 234027.

[10] Rettenmeier, M., Möller, M., Bocksrocker, O., Salvarrajan, V., Neugebauer, C., 2023. Battery recycling – Exploitation of laser technologies for dismantling and recycling processes.

[11] Saxena, P., Shukla, P., 2021. A comprehensive review on fundamental properties and applications of poly(vinylidene fluoride) (PVDF). Adv Compos Hybrid Mater 4, 8–26.